Boron Position-Dependent Surface Reconstruction and Electronic States of Boron-Doped Diamond: An Ab-initio Study

SCHOLARONE™
Manuscripts

ARTICLE

Boron Position-Dependent Surface Reconstruction and Electronic States of Boron-Doped Diamond (111) Surface: An Ab-initio Study

Le The Anh[a], Francesca Celine Catalan[b], Yousoo Kim[b], Yasuaki Einaga[c], and Yoshitaka Tateyama[*a]

Boron-doped diamond (BDD) has attracted much attention in semi-/superconductor physics and electrochemistry, where the surface structures and electronic states play crucial roles. Herein, we systematically examined the structural and electronic properties of the unterminated and H-terminated diamond (111) surfaces by using density functional theory calculations, and the Boron position's effect on them. The surface energy increases to that of the undoped case when the Boron is located at a deeper position in the diamond bulk, which indicates that Boron near the surface can facilitate the surface stability of the BDD in addition to H-termination. Moreover, the surface energy and projected density of states analyses suggest that the Boron can enhance the graphitization of the pristine (ideal) unterminated (111) surface thanks to the alternative sp^2-sp^3 arrangement in that surface. Finally, we found that surface electronic states depend on the Boron's position, i.e., the Fermi energy (E_F) is located around the mid-gap position when the Boron lies near the surface, instead of showing a p-type semiconductor behavior where the E_F lies closer to the valence band maximum (VBM).

1. Introduction

Nowadays, diamond is becoming a promising material for a wide range of applications as superconductor[1-5] and as an electrode[6-12]. Superconductivity of heavily boron-doped diamond (BDD) was intensively discussed to be bulk type II superconductor[1-4]. For the impurity states, the Hydrogen, Nitrogen and Boron are three common dopants and substitutional Boron was considered to bring a dangling bond on the sp^3 Carbon atoms[5]. However, on the surface where the sp^2 Carbon mixes up with the sp^3 Carbon, the role of Boron should be re-considered. Therefore, the stability of the BDD reconstructions, as well as surface electronic properties, is still unclear. Experimentally, there is a technical difficulty of high-resolution surface measurements of BDD, which limits the experimental confirmation of the BDD surface structures, as well as the heterogeneity of the diamond surface reconstructions brought by different growth and doping conditions[7, 8, 13-25].

Many theoretical studies proposed various reconstructions of the diamond surfaces[26-47]. For the (100) surface, the (100)-p(2x1) was predicted as the most stable surface[29, 30, 33, 37, 40]; In addition, Hong proposed dihydride configurations on diamond (100) and concluded that the canted/tilted (100)-(1x1):2H

dihydride phase has the lowest energy among the dihydride structures[36]. For the BDD (111), three reconstructions were widely accepted: pristine (111)-(1x1), single chain (111)-(2x1)-SC, and Pandey chain (111)-(2x1)-PC[40-47]. In addition, both monohydride and dihydride terminations on the (111) surfaces were discussed as possible reconstructions[41, 42]. However, a comprehensive comparison of these reconstructions is still missing and the surface reconstruction energetics remains to be an open question, which is crucial to identify the surface features under various experimental conditions. Moreover, the impact of the Boron on the stability and graphitization of the BDD (111) are still debated[48]. The relevance of the expected p-type semiconductor electronic feature of BDD has been a matter of discussion as well[49].

In this paper, we classify the reconstruction stability, via energy comparison, and the surface electronic properties of the diamond (111) surfaces with the unterminated, monohydride, and dihydride terminations using density functional theory (DFT)-based first-principles geometry optimizations. First, we examine the H-termination effect on the stability and electronic states of the (111) surfaces. Then, we study the impact of the Boron's position on the surface stability and electronic properties using a sufficiently large supercell consisting of 16 monolayers of Carbon, compared to Ref.[49]. With the present calculations, we finally discuss the mechanism of the Boron's position dependence of the surface reconstruction stability and the electronic states variation between the surface states and the bulk acceptor states.

a. Center for Green Research on Energy and environmental Materials (GREEN) and International Center for Materials Nanoarchitectonics (MANA), National Institute for Materials Science (NIMS), 1-1 Namili, Tsukuba, Japan: E-mail. TATEYAMA.Yoshitaka@nims.go.jp

b. Surface and Interface Science Laboratory, RIKEN, 2-1 Horosawa, Wako, Saitama 351-0198, Japan.

c. Department of chemistry, Keio University, 3-14-1 Hiyoshi, Yokohama 22308522, Japan.

2. Calculation methods

In search for metastable surface reconstruction structures, we use DFT calculations with the PBE[50] exchange-correlation functional implemented in the CPMD package[51]. The norm-conserving Goedecker pseudopotential[52] is used with 90 Ry cutoff energy. We apply 2x2x1 Monkhorst-Pack K-mesh to all supercells during the geometry optimizations. The systems are optimized by the GDIIS algorithm[53, 54] with the convergence orbital of 1.0×10^{-5} a.u. and convergence geometry of 2.0×10^{-3} a.u. All calculations are carried out with spin-polarized scheme because of the presence of a Boron atom.

After the geometry optimizations, we carry out post-SCF calculations with 6x6x1 K-mesh to obtain total energy and projected density of states (PDOS). In particular, we use PAW-PBE exchange-correlation with 400 eV cutoff energy implemented in VASP package[55-58]. All geometry optimizations and the SCF calculations include van der Waal correction vdW-D2[59]. Supercells with 128 Carbon atoms are used to model the (111) surfaces (dimension: 8.77 Å x 5.06 Å x 50.28 Å). The Z-axis is chosen to be about three times the thickness of the diamond slabs (16 mono-layers of Carbon atoms ~ 17 Å). Boron doping was represented by one boron dopant atom per 128 Carbon atoms (~0.7%). We terminate Hydrogen atoms to all bottom surfaces of the slabs.

The surface energy E_s is defined as:

$$E_s = \frac{E_{tot} - \sum \mu_i n_i}{N} \qquad (1)$$

Where E_{tot} is total energy of the slab, μ_i is standard chemical potential of the Carbon, Hydrogen and Boron, n_i is the number of atoms, and N is the number of the topmost surface atoms of the slab. For the unterminated and monohydride surfaces, the number of surface atoms is 8 while that of dihydride surfaces is 16. The standard chemical potential of Carbon, Hydrogen and Boron are -9.09 eV, -3.34 eV, and -5.40 eV, respectively. We consider bulk diamond, isolated H_2 molecule, and neutral Boron atom at a lattice site of a bulk diamond to calculate the chemical potentials.

3. Results and Discussions

Diamond surface reconstructions

We re-explored the atomistic pictures of the reconstructed diamond (111) surfaces as shown in Figure 1. All the optimized (111) surfaces were reported in previous DFT papers[40-47]. They are pristine (or ideal in other publications) (111)-(1x1), single chain (SC) labelled as (111)-(2x1)-SC, Pandey chain (PC), denoted as (111)-(2x1)-PC. For brevity, we refer to these structures in the manuscript as (1x1), SC, and PC, respectively. We compare the dimer lengths of the unterminated surface (0H), monohydride surface (1H), and dihydride surface (2H). The dihydride Pandey chain is not stable in geometry optimizations. The dimer lengths of the unterminated (1x1):0H and monohydride (1x1):1H are 1.48 Å and 1.54 Å, respectively. The H-termination only elongates the dimer length of the pristine

(1x1) structure by 0.06 Å. For the Pandey chain, the dimer lengths of the top chain are 1.44 Å (unterminated) and 1.57 Å (monohydride); the dimer lengths of the lower chain are 1.56 Å (unterminated) and 1.60 Å (monohydride). For the single chain, the dimer lengths of the chains are 1.46 Å, 1.54 Å, and 1.52 Å for the unterminated, monohydride, and dihydride structure, respectively. Overall, the H-termination increases the dimer lengths of the chains by about 0.1 Å compared to the
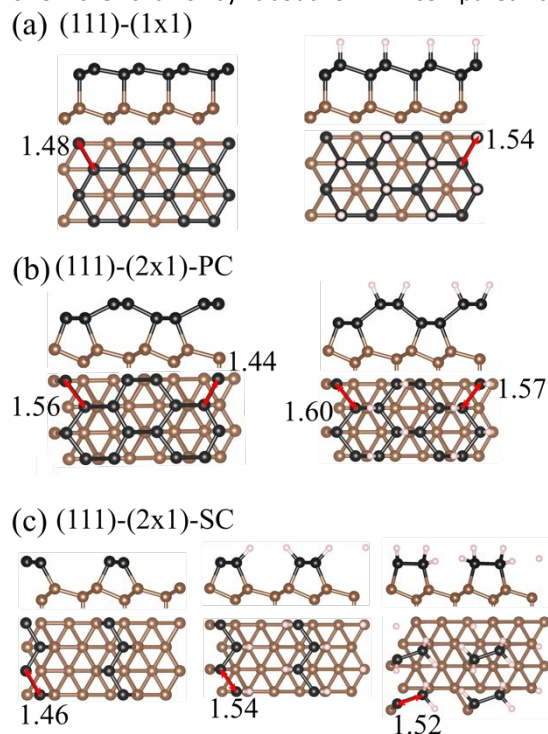
Fig. 1 Atomistic reconstructions side- and top-views of the BDD (a) pristine (111)-(1x1) without H-termination (left) and with monohydride (right); (b) Pandey chain (111)-(2x1)-PC without H-termination (left) and monohydride (right); (c) Single chain (111)-(2x1)-SC without H-termination (left), monohydride (middle) and dihydride (right). The black and brown spheres denote surface Carbon and the other Carbon, respectively. Hydrogen atoms are shown by white spheres. The values are bond lengths in (Å).

corresponding unterminated structure.

We then report the surface energy in Table 1. The lowest-energy structure is the pristine monohydride (1x1):1H. The unterminated Pandey chain PC:0H is 1.56 eV/site higher than (1x1):1H. The SC:0H and (1x1):0H are significantly higher in energy by about 2.81 eV/site and 2.32 eV/site compared to the (1x1):1H, respectively. For the dihydride structure SC:2H, it has 1.12 eV/site higher energy than the pristine monohydride. Our results suggest that the unterminated Pandey chain is the most stable structure for the unterminated (111) surfaces, and therefore should dominate such surface in experiments.

On the other hand, the pristine monohydride (1x1) has the lowest surface energy for H-terminated surfaces, which is consistent with previous studies[26, 47]. The surface energy of the monohydride Pandey chain PC:1H is 0.65 eV/site higher than that of the pristine one. The SC:1H has a higher surface energy than the (1x1):1H by about 0.34 eV/site. We also found that the surface energies of all the monohydride structures are negative while the unterminated and dihydride structures are positive,

which indicates the superiority of the monohydride structures. Interestingly, the monohydride SC:1H is more stable than the PC:1H by 0.31eV/site, which suggests the possibility of finding SC:1H in experiments. Under H-rich condition, there might be a possibility of the appearance of the dihydride SC:2H with 0.33 eV/site.

Table 1 Calculated surface energies E_s per site of the unterminated (0H), monohydride (1H), and dihydride (2H) of the undoped diamond (111) surfaces.

Surfaces	E_s (eV/site)
pristine (1x1):0H	1.53
Pandey PC:0H	0.77
Single SC:0H	2.02
pristine (1x1):1H	-0.78
Pandey PC:1H	-0.13
Single SC:1H	-0.44
Single SC:2H	0.33

Projected density of states

We then examined the surface electronic states of the above diamond surfaces. In Ref.[49], the unterminated Pandey chain structure is discussed for the X-ray spectra showing the gap states in a BDD sample, in which is Fermi level is located just above the valence band maximum. However, there are other possibilities to explain the spectra. In addition, our preliminary Scanning Tunneling Microscopy measurement implies that the Fermi level is located in the mid-gap states in some BDD surfaces. Therefore, a comprehensive survey of PDOS is still necessary.

We used the PBE+vdW-D2 functional, giving a band gap of 4.23 eV for bulk diamond, which is in agreement with the typical values by the PBE functional. For the H-terminated (111) diamond surface, the calculated PDOS gave about 2.5 eV of the band gap, which is perfectly consistent with the Ref.[44] where the surface effect slightly narrows the gap. Therefore, we can discuss the calculated electronic states (the band gap and the surface states) reasonably, taking the typical gap underestimation via PBE into account.

Figure 2 shows the calculated PDOSs for the undoped diamond (111) surfaces with various H-terminations: without H-termination, monohydride, and dihydride. We consider all Carbon atoms within 5 Å below the topmost atom, effectively involving the top 5 monolayers, as surface Carbon atoms. In Figure 2, we show the summations of the PDOSs on these surface Carbon atoms decomposed into s- and p-orbitals. These show the dominant contribution of the p-orbital in the surface Carbon atoms to the surface-states as well as other states in the valence and conduction bands. We can see from Figure 2 that there are surface states in the mid-gap of the unterminated structures while there are virtually no surface states in the H-terminated structures, implying that the surface states are due to dangling bonds. Interestingly, only the unterminated surface of the pristine (1x1):0H shows the position of the Fermi level at the mid-gap while the Fermi levels in the unterminated Pandey chain PC:0H and unterminated single chain SC:0H stay near the

VBM. Overall, we observe surface states in the unterminated (111) surfaces and that the surface energies of these surfaces are about 2-3 eV/site higher in energy than the monohydride cases (the lowest energy structures). For the H-terminated surfaces, the surface states disappear and the bandgaps are about 2~2.5 eV for the monohydride cases. The bandgap for the dihydride SC:2H is about 2.2 eV, which is smaller than the monohydride case by about 10%. In general, the substantial
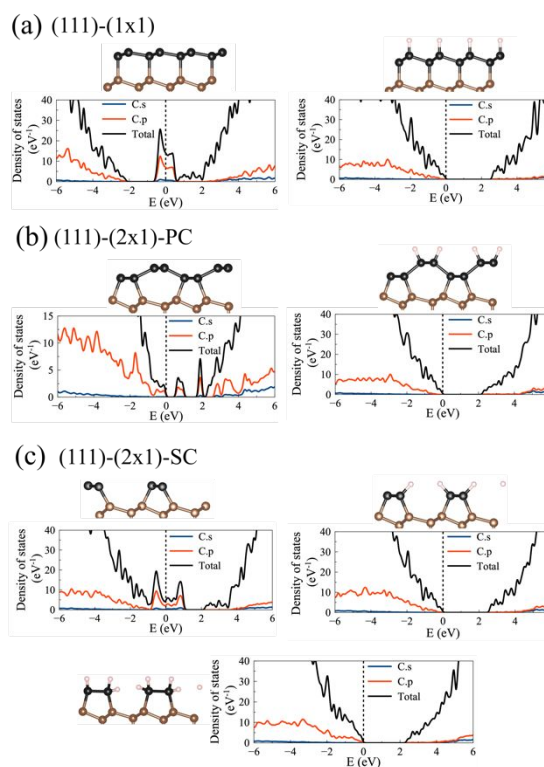
Fig. 2 Projected density of states (PDOS) for the (a) pristine (111)-(1x1), (b) Pandey chain (111)-(2x1)-PC, and (c) single chain (111)-(2x1)-SC surfaces without H-termination and with H-terminations. The total DOS is plotted with s-, p-decomposed orbital PDOS of the surface Carbon atoms. Energy origin is set to the orbital energy of the highest occupied states.

band-gaps are expected in the stable diamond surfaces with H-termination. Moreover, there are theoretical and experimental studies[60-62] suggesting that a graphene layer can be formed on the undoped diamond (111) surface under high temperature, which may induce the mid-gap states. In addition to that, the roles of Boron on the surface stability, the electronic surface states and the graphitization of the diamond (111) surface are still mattering of great interest. Below, we will discuss the Boron's position effect on the BDD (111) surface.

The impact of the Boron's position on the surface states of the BDD (111)

Here we focus on the dependence of the surface structures and surface electronic states on the location of the Boron dopant. For the H-terminated surface, we calculate the PDOS of the monohydride (1x1):1H, PC:1H, and SC:1H and found that there are no surface states and the PDOS does not depend on the Boron's position (See the Supporting Information). It is also

confirmed that the Fermi level always stays at the VBM regardless of the Boron's position in all H-terminated structures. In addition, the surface energy does not vary much as a function of the Boron's position as indicated in Table S3 (Supporting Information).

To elucidate the possible surface relaxation and graphitization, we examined two unterminated surfaces: the pristine (1x1):0H (Figure 3) and the intermediate structure graphene-on-diamond (1x1)-gr:0H (Figure 4). The results for the other surfaces can be found in the Supporting Information (Figure S3-S8). The graphitization of the diamond (111) surface was discussed based on either the Pandey chain PC:0H[60] or pristine (1x1):0H[61]. In fact, there are theoretical and experimental literatures[60, 62] suggesting that the pristine undoped structure (1x1):0H may experience the intermediate structure (1x1)-gr:0H before the graphene layer completely detaches from the diamond (111) surface. For the Boron-doped case, the role of

Fig. 3 Density of states (DOS) of B-doped (111)-(1x1):0H surfaces (a-g) in comparison with the undoped case (h). The position of the Boron atom (green ball) is changed from the 1st layer (a) to the 7th layer (g).

Boron was discussed based on the total energy to enhance the graphitization of the diamond (111) surface[48] but the detailed mechanism has not been well established.

The surface energies of the two structures are reported in Table 2. The surface energy significantly decreases with the presence of Boron at the sub-surface layers. The surface energy increases from the surface Boron (1st-6th layers) to the bulk Boron (7th layer), indicating that Boron prefers to stay in the sub-surface layers rather than in bulk. In Table 2, we report the surface energy of the Pandey chain and single chain as well. The Pandey chain surface has the lowest surface energy (~0.3 eV/site)

compared to the single chain (~2 eV/site), pristine (~1.5 eV/site), and intermediate graphene-on-diamond (~1.0 eV/site). The present result clearly shows that surface Boron can stabilize the unterminated surface of the BDD (111). Boron has little effect on the PC:0H because the surface energy only slightly varies with the Boron's positions. On the other hand, the surface energy is significantly reduced for the (1x1):0H, (1x1)-gr:0H, and SC:0H structures when the Boron is at sub-surface layers.

Table 2 Calculated surface energies per surface site (Es) of the unterminated structures: (1x1):0H and the graphene-on-diamond structure (1x1)-gr:0H in comparison with the PC:0H and SC:0H with various Boron's positions

Surfaces	(1X1):0H E_s (eV/site)	(1X1)-gr:0H E_s (eV/site)	PC:0H E_s (eV/site)	SC:0H E_s (eV/site)
undoped	1.53	1.09	0.38	2.02
B at 1st layer	1.18	0.74	0.31	1.74
B at 2nd layer	1.29	0.81	0.32	1.75
B at 3rd layer	1.18	0.75	0.34	1.77
B at 4th layer	1.31	0.86	0.34	1.91
B at 5th layer	1.29	0.90	0.34	1.96
B at 6th layer	1.34	0.93	0.36	1.98
B at 7th layer	1.39	0.98	0.36	1.99

Regarding the graphitization, we can see from Table 2 that at the same Boron's position, the surface energies of the (1x1)-gr:0H are always smaller than those of the pristine (1x1):0H. We suggest that Boron can enhance the graphitization of the pristine (1x1):0H surface.

As for the electronic states, Figure 3 shows the PDOS of the pristine (1x1):0H surface with various Boron's positions. The Fermi level is located near the VBM when the Boron is at the 7th layer. All the surface states are pinned to the E_F near the VBM which is associated with the acceptor character of the bulk
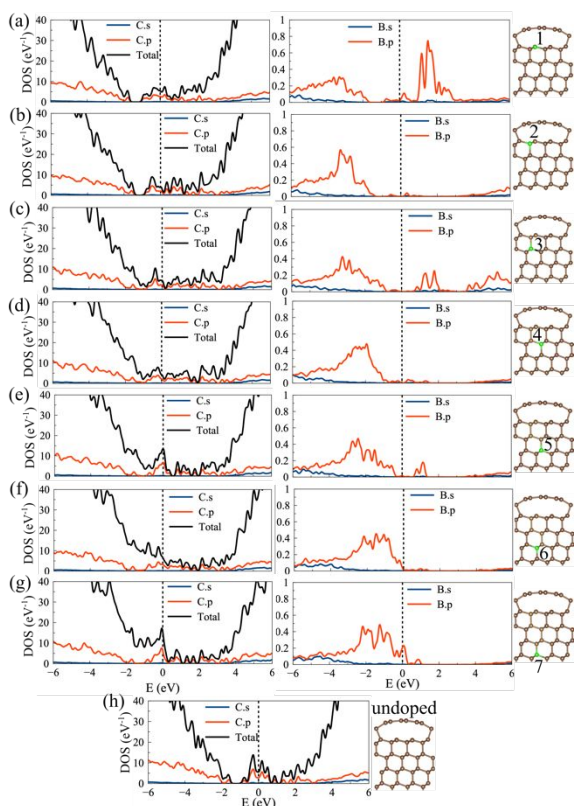
Fig. 4 Density of states of undoped and B-doped graphene-on-diamond (111)-(1x1)-gr:0H surfaces (a-g) in comparison with the undoped case (h). The position of the Boron atom (green ball) is changed from the 1st layer (a) to the 7th layer (g).

Boron, leaving a clear bandgap as can be seen in Figure 3. Consequently, we observe that the surface states remain but the position of the Fermi level significantly changes from the mid-gap to the VBM as the Boron's position changes from the topmost layer to the bulk layer (the 7th layer). The surface electronic states in this structure are mainly contributed by dangling bonds. Moreover, the Boron-specific PDOS indicate the dependence of the peaks emerging around 2 eV above the E_F when the Boron is in the odd layers (1st, 3rd, 5th) and suddenly disappear for the case when the Boron stays in the even layers (2nd, 4th, 6th). From the 7th layer, these peaks disappear regardless of whether it is in an odd or even layer. We suggest that the electronic charge density in the pristine surface (1x1):0H has an alternative sp²-sp³ layer dependence: such that the PDOS peaks around 2 eV above the E_F for when the Boron is at the odd layers (1st, 3rd, 5th) correspond to the related C-C π* characteristics (related sp² bonds) which was also investigated in a previous study[49], while the PDOS of the even layers (2nd, 4th, 6th) correspond to the bulk sp³ properties because the sp³ bond does not create mid-gap states. The origin of the surface states in this structure, thus, is mainly attributed to dangling bonds and the related sp² bonds. In previous study[42], the effect of

Boron was discussed within the interaction between the Boron and the sp³ Carbons. Presence of the sp² Carbons in the unterminated surfaces in our calculation suggests that Boron's effect can be induced with the presence of sp² Carbon as shown in Fig. 3.

For the intermediate surface (1x1)-gr:0H in Figure 4, the undoped case also surely has surface states. When the Boron is located in the topmost five layers, the Fermi level stays in the mid-gap. These Boron atoms can be regarded as the surface Boron. When the Boron atom is in the 6th layer, the Fermi level starts to be closer to the VBM, suggesting the bulk Boron. Interestingly, unlike the pristine (1x1):0H surface (Figure 3), the energy levels of the surface states in the intermediate structure still remain at mid-gap regardless of the Boron's position. We suggest that the related sp² bonds may be strongly affected due to the presence of the graphene layer which is the origin of the mid-gap states regardless the Fermi level's position in this structure. PDOS calculations indicate two possibilities for the origin of the surface states with the Fermi level at the mid-gap: either the dangling bonds of the unterminated pristine (1x1):0H which can be induced by the surface Boron or the related sp² states which are strongly affected by the presence of the
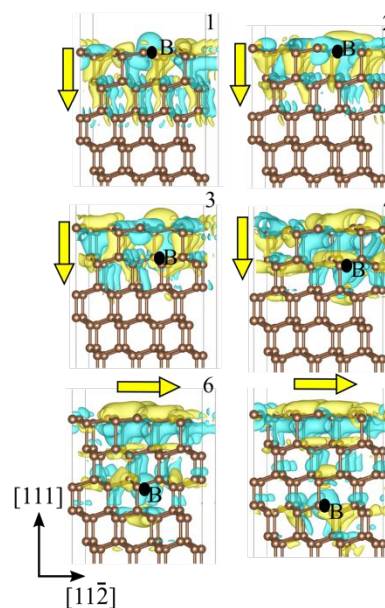
Fig. 5 The dependence of the charge density difference of the Boron's position in the B-doped (1x1):0H with respect to the undoped (1x1):0H. The iso-value is fixed at 0.005 (e/Bohr³). The yellow and cyan represent the increase and decrease of the charge density, respectively. The number indicates the layer containing the Boron atom (black dot). The arrows indicate the directions of the increase of the charge density for eye-guide.

graphene layer in the (1x1)-gr:0H structure. In both cases, the Fermi level gradually shifts from the mid-gap to the VBM when the Boron's position changes from the surface to the bulk. This behaviour is only observed with sufficient slab's thickness (16 Carbon layers in our models). For the cases of the unterminated PC:0H and SC:0H, the Fermi level always stays near the VBM regardless of the Boron's position (see Figure S3, S4 Supporting

ARTICLE

Information). The Fermi level's position and Boron's position effect clarified in this paper may be a guidance for the further study of graphitization on the BDD (111) surface. The weak influence of Boron on the surface states in this structure suggests that Boron weakly contribute to the graphene adhesion which is in agreement with previous study[43].

In addition, to clarify the mechanism of how the surface Boron stabilizes the (1x1):0H surface, we analyse the charge density difference of the B-doped (1x1):0H with respect to the undoped case ($\rho(B-doped) - \rho(Undoped)$) in Figure 5. The cyan and yellow colours indicate the decrease and increase of the charge density of the B-doped structure compared to the undoped case. We can see that the surface Boron (1st-4th layer) enhances the charge density along the [111] direction (yellow arrows) while the bulk Boron (6-7th layer) enhances the charge density mostly along the [$11\bar{2}$] direction (yellow arrows). The referenced charge distribution of the undoped surface ($\rho(Undoped)$) is shown in Figure S9 Supporting Information. Finally, we report in the Supporting Information our additional calculations for the diamond (100) surfaces. The surface reconstructions, surface energies and PDOS can be found in Figure S1, Table S1 and Figure S2, respectively.

Conclusions

We systematically investigate the various low-energy reconstructions of the diamond (111) surfaces using density functional theory. We examined several low-energy reconstructions: three monohydride surfaces: (1x1):1H, PC:1H, SC:1H and one dihydride surface: SC:2H in comparison with the corresponding unterminated surfaces. The monohydride structures are the most stable ones, SC:1H is more stable than PC:1H. The dihydride structure is about 1.12 eV/site higher in energy which may exist in the H-rich condition.

We found that instead of H-termination, Boron doping can reduce the surface energy also. The surface states of the BDD (111) surfaces can be explained by either the dangling bonds of the pristine (1x1):0H induced by the surface Boron or the related sp^2 induced by the graphene layer in the graphene-on-diamond (1x1)-gr:0H structure. Unlike the dangling bonds which is pinned to the Fermi level, the related sp^2 bonds with the presence of a graphene layer remain at the mid-gap regardless of the Fermi level's position which suggests a unique electronic property of the graphene-on-diamond structure.

Our surface energy and PDOS analyses suggest that Boron can enhance the graphitization of the pristine (1x1):0H surface thanks to the alternative sp^2-sp^3 arrangement in that surface. Manipulation of the Boron's position thus can control the surface functions of the BDD in addition to the surface termination.

Author Contributions

Y.T., Y.A. and Y.K. designed the research, L. T. A. performed the research, L. T. A., F. C. C., Y.K., Y.E., and Y.T. analysed the data and wrote the paper.

Conflicts of interest

The authors declare no competing interests.

Acknowledgements

Notes and references

1   E. A. Ekimov, V. A. Sidorov, E. D. Bauer, N. N. Mel'nik, N. J. Curro, J. D. Thompson, S. M. Stishov. *Nature.* 2004 **428**, 542–545.
2   G. Zhang, T. Samuely, N. Iwahara, J. Kačmarčík, C. Wang, P. W. May, J. K. Jochum, O. Onufriienko, P. Szabó, S. Zhou, P. Samuely, V. V. Moshchalkov, L. F. Chibotaru, H. G. Rubahn. *Sci. Adv.* 2020 **6**, eaaz2536.
3   K. Ishizaka, R. Eguchi, S. Tsuda, T. Yokoya, A. Chainani, T. Kiss, T. Shimojima, T. Togashi, S. Watanabe, C. T. Chen, C. Q. Zhang, Y. Takano, M. Nagao, I. Sakaguchi, T. Takenouchi, H. Kawarada, S. Shin. *Phys. Rev. Lett.* 2007 **98**, 047003.
4   Y. Sakai, J. R. Chelikowsky, and M. L. Cohen. *Phys. Rev. Materials* 2020 **4**, 054801.
5   F. S. Gentile, S. Salustro, G. Di Palma *et al. Theor. Chem. Acc.* 2018 **137**, 154.
6   C. Yamaguchi, K. Natsui, S. Iizuka, Y. Tateyama, Y. Einaga. *Phys. Chem. Chem. Phys.* 2019 **21**, 13788–13794.
7   Y. Einaga. *J. Appl. Electrochem.* 2010 **40**, 1807–1816.
8   Y. Einaga. *Bull. Chem. Soc. Jpn.* 2018 **91**, 1752–1762.
9   S. Kasahara, T. Ogose, N. Ikemiya, T. Yamamoto, K. Natsui, Y. Yokota, R. A. Wong, S. Iizuka, N. Hoshi, Y. Tateyama, Y. Kim, M. Nakamura, Y. Einaga. *Anal. Chem.* 2019 **91**, 4980–4986.
10 T. A. Ivandini, Y. Einaga. *ChemComm.* 2017 **53**, 1338–1347.
11 C. Comninellis, A. Kapalka, S. Malato, S. A. Parsons, I. Poulios, D. Mantzavinos. *J. Chem. Technol. Biotechnol.* 2008 **83**, 769–776.
12 M. A. Q. Alfaro, S. Ferro, C. A. Martínez-Huitle, Y. M. Vong. *J. Braz. Chem. Soc.* 2006 **17**, 227–236.
13 T. Ando, I. Sakaguchi, K. P. Loh. *Phys. Rev. B: Condens. Matter Mater. Phys.* 1999 **59**, 10347–10350.
14 N. Lvova, A. Ryazanova, O. Ananina, A. Yemelianova. *Diam. Relat. Mater.* 2017 **75**, 110–115.
15 R. Hoffmann, A. Kriele, H. Obloh, J. Hees, M. Wolfer, W. Smirnov, N. Yang, C. E. Nebel. *Appl. Phys. Lett.* 2010 **97**, 052103.
16 M. Nimmrich, M. Kittelmann, P. Rahe, A. J. Mayne, G. Dujardin,

A. Von Schmidsfeld, M. Reichling, W. Harneit, A. Kühnle. *Phys. Rev. B: Condens. Matter Mater. Phys.* 2010 **81**, 201403(R).

17 Y. L. Yang, L. M. Struck, L. F. Sutcu, M. P. D'Evelyn. *Thin Solid Films.* 1993 **225**, 203–211.

18 G. Bogdan, M. Nesládek, J. D. Haen, J. Maes, V. V. Moshchalkov, K. Haenen, M. D'Olieslaeger. *Phys. Status Solidi A.* 2005 **202**, 2066–2072.

19 K. P. Loh, X. N. Xie, Y. H. Lim, E. J. Teo, J. C. Zheng, T. Ando. *Surf. Sci.* 2002 **505**, 93–114.

20 K. Bobrov, G. Comtet, L. Hellner, G. Dujardin, A. Hoffman. *Appl. Phys. Lett.* 2004 **85**, 296-298.

21 E. C. Sowa, G. D. Kubiak, R. H. Stulen, M. A. Van Hove. *J. Vac. Sci. Technol. A.* 1988 **6**, 832–833.

22 Th. Kohlerm, M. Sternberg, D. Porezag, Th. Frauenheim. *Phys. Status Solidi A.* 1996 **154**, 69-89.

23 H. Kawarada. *Surf. Sci. Rep.* 1996 **26**, 205–206.

24 J. Chevallier, D. Ballutaud, B. Theys, F. Jomard, A. Deneuville, E. Gheeraert, F. Pruvost. *Phys. Status Solidi A.* 1999 **174**, 73–81.

25 S. Walter, J. Bernhardt, U. Starke, K. Heinz, F. Maier, J. Ristein, L. Ley. *J. Phys. Condens. Matter.* 2002 **14**, 3085–3092.

26 K. Larsson. Simulation of Diamond Surface Chemistry: Reactivity and Properties. *Some Aspects of Diamonds in Scientific Research and High Technology, Evgeniy Lipatov, IntechOpen.* **2019**.

27 M. W. Kelly, S. C. Halliwell, W. J. Rodgers, J. D. Pattle, J. N. Harvey, M. N. R. Ashfold. *J. Phys. Chem. A.* 2017 **121**, 2046–2055.

28 K. Larsson. *C.* 2020 **6**, 22.

29 S. H. Yang, D. A. Drabold, J. B. Adams. *Phys. Rev. B: Condens. Matter Mater. Phys.* 1993 **48**, 5261–5264.

30 A. Cheesman, J. N. Harvey, M. N. R. Ashfold. *J. Phys. Chem. A.* 2008 **112**, 11436–11448.

31 Y. Song, K. Larsson. *J. Phys. Chem. C.* 2015 **119**, 2545–2556.

32 D. Petrini, K. Larsson. *J. Phys. Chem. C.* 2007 **111**, 13804–13812.

33 J. Furthmüller, J. Hafner, G. Kresse. *Phys. Rev. B: Condens. Matter Mater. Phys.* 1996 **53**, 7334–7351.

34 Y. L. Yang, M. P. D'Evelyn. *J. Am. Chem. Soc.* 1992 **114**, 2796–2801.

35 D. Petrini, K. Larsson. *J. Phys. Chem. C.* 2008 **112**, 14367–14376.

36 S. Hong. *Phys. Rev. B: Condens. Matter Mater. Phys.* 2002 **65**, 153408.

37 D. Petrini, K. Larsson. *J. Phys. Chem. C.* 2007 **111**, 795–801.

38 M. M. Hassan, K. Larsson. *J. Phys. Chem. C.* 2014 **118**, 22995–23002.

39 X. M. Zheng, P. V. Smith. *Surf. Sci.* 1991 **256**, 1–8.

40 M. De La Pierre, M. Bruno, C. Manfredotti, F. Nestola, M. Prencipe, C. Manfredotti. *Mol. Phys.* 2014 **112**, 1030–1039.

41 X. M. Zheng. *Surf. Sci.* 1996 **364**, 141–150.

42 A. Scholze, W. Schmidt, F. Bechstedt. *Phys. Rev. B: Condens. Matter Mater. Phys.* 1996 **53**, 13725–13733.

43 Y. Song, K. Larsson. *Phys. Status Solidi A.* 2016 **213**, 2105–2111.

44 S. Zhao, K. Larsson. *J. Phys. Chem. C.* 2014 **118**, 1944–1957.

45 S. Zhao, K. Larsson. *Diam. Relat. Mater.* 2016 **66**, 52–60.

46 X. Wang, C. Wang, X. Shen, K. Larsson, F. Sun. *J. Phys. Condens. Matter.* 2019 **31**, 265002.

47 D. Petrini, K.Larsson. *J. Phys. Chem. C.* 2008 **112**, 3018–3026.

48 C. Lu, H. Yang, J. Xu, L. Xu, M. Chshiev, S. Zhang, C. Gu. *Carbon.* 2017 **115**, 388–393.

49 S. Choudhury, B. Kiendl, J. Ren, F. Gao, P. Knittel, C. Nebel, A. Venerosy, H. Girard, J. C. Arnault, A. Krueger, K. Larsson, T. Petit. *J. Mater. Chem. A.* 2018 **6**, 16645–16654.

50 J. P. Perdew, K. Burke, M. Ernzerhof. *Phys. Rev. Lett.* 1996 **77**, 3865–3868.

51 *CPMD v4.3.0* (4.3.0). http://www/cpmd.org

52 S. Goedecker, M. Teter. *Phys. Rev. B: Condens. Matter Mater. Phys.* 1996 **54**, 1703–1710.

53 P. Császár, P. Pulay. *J. Mol. Struct.* 1984 **114**, 31–34.

54 Ö. Farkas, H. B. Schlegel. *J. Chem. Phys.* 1999 **111**, 10806–10814.

55 G. Kresse, J. Hafner. *Phys. Rev. B: Condens. Matter Mater. Phys.* 1993 **47**, 558–561.

56 G. Kresse, J. Furthmüller. *Comput. Mater. Sci.* 1996 **6**, 15–50.

57 G. Kresse, J. Furthmüller. *Phys. Rev. B: Condens. Matter Mater. Phys.* 1996 **54**, 11169–11186.

58 D. Joubert. *Phys. Rev. B: Condens. Matter Mater. Phys.* 1999 **59**, 1758–1775.

59 J. S. Grimme, *J. Comp. Chem*. 2006 **27**, 1787.

60 A. De Vita, G. Galli, A. Canning, R. Car. *Nature.* 1996 **379**, 523–526.

61 G. Jungnickel, D. Porezag, Th. Frauenheim, M. I. Heggie, W. R. L. Lambrecht, R. Segall, J. C. Angus. *Phys. Status Solidi A.* 1996 **154**, 109-125.

62 N. Tokuda, M. Fukui, T. Makino, D. Takeuchi, S. Yamsaki, T. Inokuma. *Jpn. J. Appl. Phys.* 2013 **52**, 110121.